International Journal of Engineering

Journal Homepage: www.ije.ir

Predictive Modelling and Optimization of Double Ring Electrode Based Cold Plasma Using Artificial Neural Network

S. K. Bhat, G. D. Deepak*

Department of Mechanical and Industrial Engineering, Manipal Institute of Technology, Manipal Academy of Higher Education, Manipal, Karnataka, India

PAPER INFO

Paper history:
Received 11 July 2023
Received in revised form 14 August 2023
Accepted 26 August 2023

Keywords:
Artificial Neural Network
Cold Plasma
Machine Learning
Biomedical Devices
Desirability Function Analysis
Ring Electrode

ABSTRACT

Cold Atmospheric Pressure Plasma (CAP) is very potent and impactful technology implemented for both technological and biomedical applications. This paper focuses on the implementation of artificial neural network (ANN) for a novel double ring electrode based cold atmospheric pressure plasma which is to operated only in the glow discharge region for its application in biomedical field. ANN inherently helps in visualizing the effective output parameters such as peak discharge current, power consumed, jet length (with sleeve) and jet length (without sleeve) for given set of input parameters of supply voltage and supply frequency using machine learning model. The capability of the ANN model is demonstrated by predicting the output parameters of the CAP beyond the experimental range. Finally, the optimized settings of supply voltage and supply frequency will be determined using the composite desirability function approach to simultaneously maximize the peak discharge current, jet length (with sleeve) and jet length (without sleeve), and minimize the power consumption.

doi: *10.5829/ije.2024.37.01a.08*

1. INTRODUCTION

Plasma is considered the fourth state of matter and is considered as ionized gas (1). Plasma is generated due to the association of strong electromagnetic field, gas and heat. Generally, reactive nitrogen and oxygen species (RONS) (2) have a main role in atmospheric pressure plasma formation (APP). As the key components of air are oxygen and nitrogen, reactive oxygen species (ROS) comprise of hydroxide and oxygen radicals, while nitrogen oxides are included as reactive nitrogen species (RNS) (3). The APP generates neutral reactive species, free electron, atom such as oxygen (O) and molecules, radicals and nitrogen oxide (NO) (4-6). Cold atmospheric pressure plasma (CAP) is applications in many fields such as: sterilization (6), surface modification (7), food safety (8), water purification (9), textiles (10), medical (11) and others. The effect of CAP is very unique and it is for specific application.

Amongst the various technologies implemented for generating atmospheric cold plasma, there are two major categories which are dominant in clinical and preclinical research in the field of plasma medicine which includes plasma jets (12-15) and dielectric barrier discharge (DBD) (16, 17). In DBD's the plasma is ignited in the gap between the powered and ground electrode. There are various types of DBD's such as volume DBD, Surface DBD used for various applications. The plasma jet experimental typically comprises of tube-like structure such as quartz tube, the plasma is generated using a working gas such as argon that would flow inside this tube. There are various electrode designs such as DBD-like jets, DBD jets and single electrode jets. The gas flow inside the quartz tube enables the resulting plasma to be carried out and is focused on the target material to be treated. Mostly noble gases are used as working gases for the generation of plasma jet.

ANN has been applied successfully in plasma medicine; Lin et al. (18) implemented ANN approach for predicting gas compositions and gas temperature using spontaneous emission spectroscopy, wherein the ANN output is used to control the power consumption of the

*Corresponding Author Email: *divya.deepak@manipal.edu* (G. D. Deepak)

Please cite this article as: Bhat SK, Deepak GD. A New Comprehensive Model for Integrating Environmental, Economic, and Social Performance of Deep and Large-scale Open-Pit Copper Mines. International Journal of Engineering, Transactions A: Basics. 2024;37(01): 83-93.

device and gas injection rate, thereby optimizing the plasma chemistry. Furthermore, Wan et al. (19) implemented an ANN model to predict NO conversion by DBD in the $N_2/O_2/NO$ system. Their ANN model results indicated that the primary factor influencing the production of NO_2 is the concentration of NO at the inlet, responsible for 36.22% of the effect. The other factors that impacted NO_2 production were discharge power at 23.52% and residence time at 26.25 %.

The cold plasma technology involves various important operating parameters, viz., supply voltage (SV), supply frequency (SF), pulse discharge current (PDC), jet length and power consumption (P) (11). From the perspective of development of CAP devices, it is of vital importance to determine the optimum levels of input parameters of supply voltage and supply frequency to achieve the desired levels of pulse discharge current, jet length and power consumption. Furthermore, since experimental tests usually have certain limitations with respect to the range of parameters, an accurate and reliable predictive model can be useful to make performance predictions beyond the range of parameters considered in the experiments. Recently, one of the robust and popular machine learning techniques called artificial neural network (ANN) has been implemented to predict the efficiency of CAP-based technologies in terms of the input parameters towards applications such as plasma treatment and CO_2 splitting (20, 21). However, there is a paucity of research in the literature on development of predictive models for the fundamental performance characteristics such as PDC, jet length and power consumption. This paper aims to develop an ANN model for the novel double ring electrode based cold atmospheric pressure plasma using a benchmark experimental data (11) to train, test and validate the model. The robustness of the neural network to model the physics of the cold plasma device is demonstrated by making performance predictions beyond the range of the experimental data used for training the model. Finally, the well-established statistical method of desirability function analysis (DFA) will be used to perform the multi-response optimization to determine the optimum settings of the input parameters for the best performance.

2. GEOMETRY AND EXPERIMENTAL SETUP

The double ring electrode configuration (11)examined in this paper comprises of quartz tube with nozzle as shown in Figure 1. Ring electrodes are the two metal sleeves that are put on top the nozzle indicated as 3 in Figure 1. One of these electrodes is connected to supply and another electrode is grounded. The nozzle outlet diameter is 3 mm and has been indicated as 2 (see Figure 1). The working gas used Argon enters through the inlet of quartz tube indicated as 1 (see Figure 1). The outer diameter and length of quartz tube is 25 mm and 155 mm, respectively. The quartz tube thickness is 1.5 mm. The diameter and axial length of ring electrodes are 4 mm and 18 mm respectively. The ring electrodes are separated by distance of 3 mm as indicated -3 in Figure 1. A quartz sleeve of 4 mm diameter and 15 mm length was placed on the nozzle of the quartz tube (see Figure 2) to observe the length of plasma jet without the effect of surrounding air. To examine the plasma jet length without the effect of surrounding air, a quartz sleeve of 15 mm length and 4 mm diameter was placed on nozzle of quartz tube (Figure 2). Jet length was examined for both without and with quartz sleeve.

The double ring electrode implemented in this paper has been subjected to supply voltages upto 6 kV and supply frequencies upto 25 kHz. Working gas employed was Argon as shown in Figure 2. The V-I characteristic of the developed DBD-based cold plasma jet (Figure 2) has been studied and the consumption of power has been analyzed at various input combinations (supply voltage and frequency). The supply frequency and voltage have been varied from 10 to 25 kHz and 3.5 to 6 kV, respectively. The gas flow rate is fixed at 1 liter/min. The experimental results of pulse discharge current (PDC), jet length without and with sleeve (JLwoS and JLwS) and power (P), for the various supply voltage and supply frequencies is listed in Table 1.

In this paper, ANN is implemented for the experimental data as listed in Table 1 to analyze and

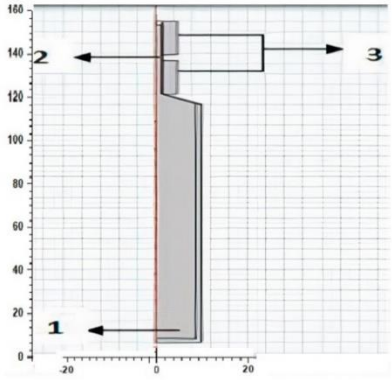

Figure 1. Geometry of double ring electrode based cold plasma jet using Argon

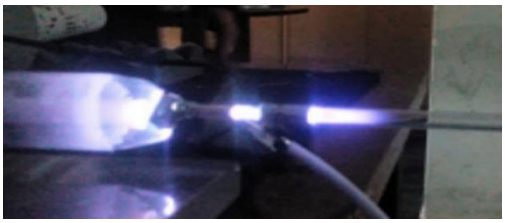

Figure 2. Argon based cold plasma jet using double ring electrode

TABLE 1. Experimental results [11]

Expt. No.	SV (kV)	SF (kHz)	PDC (mA)	JLwoS (mm)	JLwS (mm)	P (W)
1	3.5	10	152	2	5	0.28
2	4	10	160	4	7	0.33
3	4.5	10	176	7	9	0.46
4	5	10	144	12	15	0.46.
5	5.5	10	176	15	21	0.56
6	6	10	192	17	22	0.42
7	3.5	15	96	4	7	0.33
8	4	15	112	6	9	0.58
9	4.5	15	152	8	12	0.58
10	5	15	144	14	17	0.69
11	5.5	15	176	18	23	0.78
12	6	15	232	20	24	0.63
13	3.5	20	88	6	10	0.59
14	4	20	128	8	12	0.73
15	4.5	20	112	12	15	0.82
16	5	20	152	18	22	1.12
17	5.5	20	168	20	25	1.04
18	6	20	184	22	27	0.72
19	3.5	25	88	8	12	0.94
20	4	25	96	11	14	0.89
21	4.5	25	152	12	17	0.88
22	5	25	128	22	25	0.97
23	5.5	25	144	24	28	1.27
24	6	25	216	25	29	1.04

predict the output parameters (discharge current, jet length (with and without sleeve) and power consumption for higher values of supply voltage and supply current for the double ring electrode-based argon cold plasma jet.

3. ANN APPROACH

Artificial neural network (ANN) is a soft computing paradigm which derives its functionality through inspiration from the neurons in the biological nervous systems. ANN operates with a similar principle of that of biological neurons wherein the information processing takes place in the individual neurons starting with a feedforward training process, also involving a backpropagation feedback loop to estimate the errors in prediction, to derive a mathematical formulation to model the relationship between process parameters and the output responses (22).

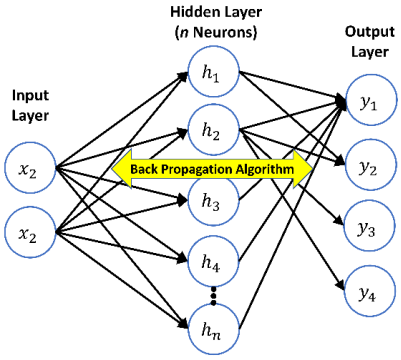

Figure 3. General architecture of a single hidden layer NN model with *n* neurons

In the simplest configuration, a neural network model consists of an input layer which consists of the input parameters, followed by a hidden layer which consists of an arbitrary number of neurons according to the requirements of the problem, and finally the output layer which is nothing but the list of the output parameters (Figure 3). In this study, a multi-layer perceptron ANN model was developed using the *fitnet* function in MATLAB (MathWorks, Natick, Massachusetts, USA). The multi-layer perception basically falls into the category of neural networks with more than one hidden layer. To ensure a good predictive accuracy of the model, the possibility of having one or more hidden layers was investigated. The Levenberg-Marquardt algorithm was employed for training the model (23). The inputs are the two control parameters, i.e., SV and SF; and the outputs are the four response parameters, PDC, JLwS, JLwoS, and P.

The input data was divided into three sets such that 70% of it was used for training and remaining 15% each were used for testing and validation of the network. Numerous trials were conducted with the number of hidden layers and the number of neurons in them to arrive at a model which provided a good descriptive performance (refer Appendix for details), which is then made use to make predictions beyond the experimental range of control parameters.

Each neuron in the artificial neural network consists of three components, weights ($w_{k,j}$), biases (b_k), and an activation function. The weights and biases are fed to individual neurons along with the inputs to obtain the mathematical operation in each neuron as Equation (1) (24):

$$U_k = b_k + \sum_{j=1}^{n} w_{k,j} \times I_j \quad (1)$$

where, n is the number of inputs and k signifies the k^{th} neurons in the hidden layer. The same equation can be written in the matrix form as Equation 2 (22):

$$U_k = \begin{pmatrix} w_{11} & \cdots & w_{1n} \\ \vdots & \ddots & \vdots \\ w_{m1} & \cdots & w_{mn} \end{pmatrix}_{m\times n} \begin{bmatrix} I_1 \\ \vdots \\ I_n \end{bmatrix}_{n\times 1} + \begin{bmatrix} b_1 \\ \vdots \\ b_n \end{bmatrix}_{m\times 1} = \begin{bmatrix} U_1 \\ \vdots \\ U_n \end{bmatrix}_{m\times 1} \quad (2)$$

The inputs and outputs in each neural network are typically normalized between $[-1, +1]$. Finally, the overall mathematical relationship to predict the output 'Y' can be written as Equation 3 (22):

$$Y = b_{output-layer} + \sum_{k=1}^{m} LW_k \times f(U_k) \quad (3)$$

where, $b_{output-layer}$ is the output layer weight and LW_k is the layer weight matrix. The activation function $f(x)$ is a tan-sigmoid (*tansig*) or hyperbolic tangent function as shown by Equation 4 (23):

$$f(U_k) = \frac{2}{1-e^{-2U_k}} - 1 \quad (4)$$

In this study, the *tansig* function was used for the connections between the input and hidden layers and the hidden layers to output layers [20-22]. The descriptive accuracy of the model was evaluated based on the coefficient of determination (R^2), which is given by Nateghi- and Ahmadi (24):

$$R^2 = 1 - \frac{\sum_{i}^{n}\left(y_i - y_{\exp-i}\right)^2}{\sum_{i}^{n}\left(y_i - \bar{y}_{\exp-i}\right)^2} \quad (5)$$

where, y_i and y_{exp-i} are the model predictions and the corresponding experimental data, respectively, and $\bar{y}_{exp-i}$ indicates the mean of the experimental response, for a particular response parameter.

4. DESIRABILITY FUNCTION ANALYSIS

Desirability Function Analysis (DFA) is a statistical method used for multi-response optimization, particularly in the field of experimental design and quality improvement. It provides a way to simultaneously optimize multiple responses or variables in a process or system. The main idea behind DFA is to convert individual response variables into a single overall desirability value.

Firstly, the individual desirability function for each factor setting is calculated. This is called as the desirability index (DI). Next, the overall desirability for a particular combination of factor settings, termed as composite desirability index (CDI), is calculated as the geometric mean of the individual desirability values. This approach ensures that all responses contribute equally to the overall desirability assessment [25-27].

$$d_i = \begin{cases} 0 & y_i < y_{\min} \\ \left(\dfrac{y_i - y_{\max}}{y_{\max} - y_{\min}}\right)^s & y_{\min} \le y_i \le y_{\max}, s \ge 0 \\ 1 & y_i > y_{\max} \end{cases} \quad (6)$$

$$d_i = \begin{cases} 1 & y_i < y_{\min} \\ \left(\dfrac{y_i - y_{\max}}{y_{\min} - y_{\max}}\right)^r & y_{\min} \le y_i \le y_{\max}, r \ge 0 \\ 0 & y_i > y_{\max} \end{cases} \quad (7)$$

The goal of DFA is to find the factor settings that maximize the overall desirability (or CDI). This can be achieved using optimization techniques such as response surface methodology. By optimizing the overall desirability, DFA helps identify the factor settings that simultaneously optimize multiple responses and improve the quality or performance of a process or system.

The principle of DFA first propounded by Harrington in 1965 (25) was refined and brought to its presently used form by Derringer and Suich in 1980 (26). The method of DFA is enunciated as follows. Firstly, based on the criteria of whether a response variable needs to be maximized (larger-the-better) or minimized (smaller-the-better), the desirability index (DI) for each factor setting combination is calculated using the Equations 6 and 7, respectively (27).

Equations 6 and 7, y_{min} and y_{max} indicate the minimum and maximum of the response y_i. The exponents s and r are the weights assigned to each response variable. Here, we assign equal weightage to all the response, implying, $s = r = 0.25$. In this study, the PDC and P were subjected to the condition of smaller-the-better, whereas the larger-the-better condition was imposed on JLwS and JLwoS. Now, the composite desirability index (CDI) is computed as follows (27):

$$CDI_i = \left(d_{i,1}^{w_1} \times d_{i,2}^{w_2} \times d_{i,3}^{w_3} \times \ldots \times d_{i,k}^{w_k}\right)^{1/k} \quad (8)$$

where, k indicates the number of responses (here, $k = 4$), $d_{i,k}^{w_k}$ represents the desirability index of the k^{th} response and w_1, w_2, w_3,…, are the weightages assigned to individual responses, such that $\sum_i^k w_i = 1$. Here, we assign equal weightage, implying, $w_i = 0.25$. Now, the mean of factor effect at each level is analyzed to obtain the best combination of the control parameters to achieve the maximum possible CDI (27). The maximum possible CDI signifies the optimized control parameter setting combination at which the multiple responses are achieving their best possible combinatorial outcome.

5. RESULTS AND DISCUSSION

5. 1. Descriptive and Predictive Modeling using Artificial Neural Network The artificial neural network for modeling the performance of the double ring electrode based cold plasma jet was developed by a trial-and-error approach by varying the number of hidden layers and the number of neurons in them. The number of layers were varied from 1 to 3, and in each layer, the

number of neurons were changed from 3 to 20. During these trials, the descriptive accuracy of the model was evaluated by means of the coefficient of determination (R^2) for each of the four performance parameters (PDC, JLwS, JLwoS and P). It was found that, a two-layered ANN with 8 and 12 neurons, in the first and second hidden layers, respectively (Figure 4), provided the best descriptive accuracy with $R^2 > 0.96$ for all the parameters. Figure 5 graphically depicts the descriptive accuracy of the ANN model for the parameters. Table 2 (Expt. No. 1 – 24) lists the numerical predictions of the ANN model for the experimental data shown in Table 1.

A robust model not only needs to accurately model the experimental data, but also make predictions for new set of data beyond the experimental range, while being consistent with the physics of the problem. After confirming the descriptive accuracy of the ANN model, its predictive capability is investigated by forecasting the performance parameters beyond the range of control parameters used in the experiments. Table 2 (Expt. No.25 – 56) shows the predictions of the ANN model for 6.5 kV ≤ SV ≤ 10 kV and 10 kHz ≤ SF ≤ 25 kHz.

The split of the datasets for training, testing and validation steps were chosen randomly in each trial using the MATLAB function dividerand, which splits the data based on random indices. For the optimum model (2-8-20-4) the expt no. 1, 3, 5, 7, 8, 9, 10, 11, 12, 13, 14, 15, 17, 18, 20, 21, 23 were used for training, expt no. 16, 29, 22, 24 were used for validation and remaining (2, 4, 6, 19) were used for testing purposes.

From Table 2, for (3 kV, 10 kHz) the power consumed in the plasma is 0.33 W with short plasma jet lengths (5.1 mm (JLwS), 2.1 mm (JLwoS)), as the energy is consumed by the seed electrons for plasma generation. Whereas, when supply voltage approaches 6 kV, 10 kHz then power consumption is 0.56 W with longer jet lengths (26.1 mm (JLwS), 20.3 mm (JLwoS)) indicating that power is utilized for plasma generation. It is also observed that plasma jet lengths with sleeve for most cases of supply voltages and frequency (3.5 kV – 10 kV,

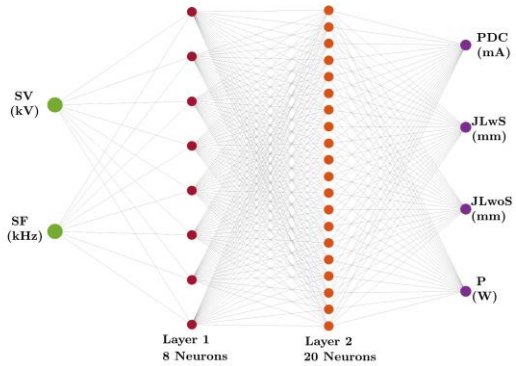

Figure 4. ANN architecture with '2-8-20-4' topology

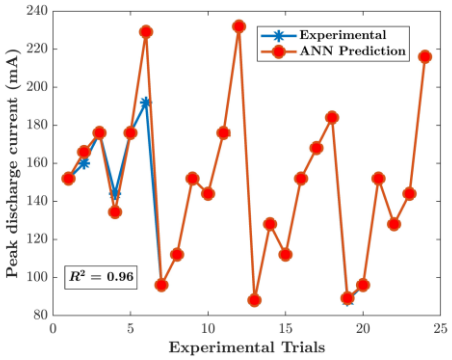

(a)

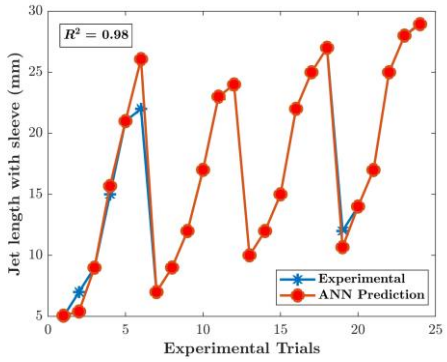

(b)

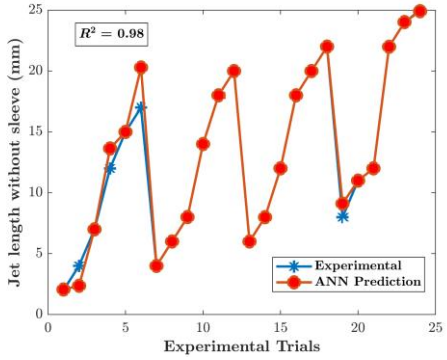

(c)

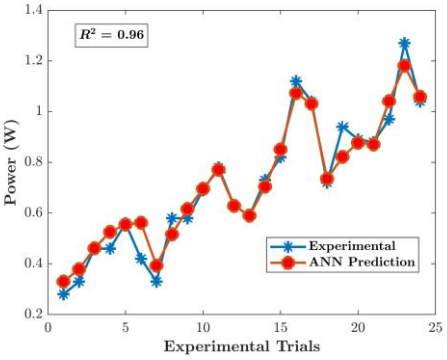

(d)

Figure 5. Comparison of ANN predictions for (a) PDC, (b) JLwS, (c) JLwoS, (d) P, with the corresponding experimental responses

TABLE 2. ANN predictions for within the range of experimental data provided in Table 1 and beyond the range of supply voltage (6 kV ≤ SV ≤ 10 kV and 10 kHz ≤ SF ≤ 25 kHz)

Expt. No.	SV (kV)	SF (kHz)	PDC (mA)	JLwoS (mm)	JLwS (mm)	P (W)
1	3.5	10	152.0	5.1	2.1	0.33
2	4	10	165.9	5.4	2.4	0.38
3	4.5	10	176.0	9.0	7.0	0.46
4	5	10	134.4	15.7	13.6	0.53
5	5.5	10	176.0	21.0	15.0	0.55
6	6	10	229.1	26.1	20.3	0.56
7	3.5	15	96.0	7.0	4.0	0.39
8	4	15	112.0	9.0	6.0	0.52
9	4.5	15	152.0	12.0	8.0	0.62
10	5	15	144.0	17.0	14.0	0.70
11	5.5	15	176.0	23.0	18.0	0.77
12	6	15	231.9	24.0	20.0	0.63
13	3.5	20	88.1	10.0	6.0	0.59
14	4	20	128.0	12.0	8.0	0.70
15	4.5	20	112.0	15.0	12.0	0.85
16	5	20	152.0	22.0	18.0	1.07
17	5.5	20	168.0	25.0	20.0	1.03
18	6	20	184.0	27.0	22.0	0.74
19	3.5	25	89.1	10.7	9.1	0.82
20	4	25	96.0	14.0	11.0	0.88
21	4.5	25	152.0	17.0	12.0	0.87
22	5	25	128.0	25.0	22.0	1.04
23	5.5	25	144.0	28.0	24.0	1.18
24	6	25	216.0	28.9	24.9	1.06
25	6.5	10	232.0	26.6	22.5	0.53
26	7	10	232.0	26.1	23.2	0.52
27	7.5	10	232.0	25.7	23.5	0.51
28	8	10	232.0	25.5	23.6	0.50
29	8.5	10	232.0	25.4	23.6	0.50
30	9	10	232.0	25.4	23.6	0.50
31	9.5	10	232.0	25.4	23.6	0.50
32	10	10	232.0	25.4	23.6	0.50
33	6.5	15	232.0	25.6	22.9	0.54
34	7	15	232.0	25.8	23.4	0.52
35	7.5	15	232.0	25.7	23.5	0.51
36	8	15	232.0	25.6	23.6	0.51
37	8.5	15	232.0	25.5	23.6	0.50
38	9	15	232.0	25.5	23.6	0.50
39	9.5	15	232.0	25.4	23.6	0.50
40	10	15	232.0	25.4	23.6	0.50
41	6.5	20	220.0	27.7	23.5	0.56
42	7	20	229.2	27.5	23.6	0.52
43	7.5	20	231.5	27.1	23.4	0.51
44	8	20	231.9	26.8	23.3	0.51
45	8.5	20	232.0	26.5	23.3	0.51
46	9	20	232.0	26.2	23.4	0.51
47	9.5	20	232.0	26.0	23.5	0.51
48	10	20	232.0	25.9	23.5	0.51
49	6.5	25	223.7	29.0	25.0	0.85
50	7	25	222.9	29.0	25.0	0.74
51	7.5	25	220.7	28.9	24.9	0.67
52	8	25	217.8	28.9	24.9	0.62
53	8.5	25	216.2	28.8	24.7	0.58
54	9	25	218.1	28.6	24.5	0.55
55	9.5	25	223.4	28.3	24.2	0.53
56	10	25	228.6	27.8	23.8	0.52

10 kHz – 25 kHz) is longer as compared to jet length without sleeve as seen in Table 2. This is because the sleeve shields the plasma jet coming out from electronegative gases such as water vapor that impede the propagation of the plasma jet. The power consumed by the plasma jet increases as the supply voltage and frequency reaches up to 6 kV, 25 kHz (1.06 W). Any higher supply voltage resulted in the power being lost in heating of dielectric tube and not utilized in the plasma generation which is clearly seen in Table 2 indicating the decrease in power consumed (0.85 W at 6.5 kV, 25 kHz).

It can be further seen from Table 2 that at higher voltages of (6.5 kV, 10 kHz – 25 kHz) there is only variation of power consumption (0.53 W – 0.85 W) by the plasma as most of the power supplied is not utilized in the plasma generation but lost in the dielectric material as thermal dissipation, leading to heating of the dielectric tube. However, at (6.5 kV, 10 kHz – 25 kHz) the plasma jet length both with and without sleeve increases (26.6 mm – 29 mm (JLwS), 22.5 mm – 25 mm (JLwoS)) with increase in supply frequency. This is due to the higher energy absorbed by the seed electrons at higher supply frequency (20 kHz – 25 kHz) resulting in longer jet lengths as seen in Table 2.

A similar result has been observed at (7.5 kV, 10 kHz – 25 kHz) where there is only slight variation in the power consumed (0.51 W – 0.67 W) due to supply power being lost in thermal dissipation of the material. Further higher voltages of 8.5 kV – 10 kV (10 kHz – 25 kHz) also show only a slight variation in the power consumption as the supply power is lost as thermal dissipation. However, at (7.5 kV, 10 kHz – 25 kHz) the plasma jet length both

with and without sleeve increases (25.7 mm – 28.5 mm (JLwS), 22.5 mm – 25 mm (JLwoS)) with increase in supply frequency. This is due to the higher energy absorbed by the seed electrons at higher supply frequencies (20 kHz – 25 kHz) resulting in longer jet lengths as seen in Table 2.

But at supply voltage of (8.5 kV – 10 kV, 25 kHz) there is hardly any variation of power consumed as seen in Table 2; in fact, the power consumed reduces from 0.58 W (8.5 kV/25 kHz) to 0.52 W (10 kV/25 kHz) due to power supply lost in thermal dissipation of dielectric material and also as the plasma discharge approaches the arc discharge region which is not suitable for biomedical applications. Due to this thermal dissipation heat loss at (8.5 kV – 10 kV, 25 kHz) it must be observed that there is a decrease in plasma jet length (28.8 mm – 27.8 mm (JLwS), 24.7 mm – 23.8 mm (JLwoS)) which is evidently indicating that the power supply is not being utilized in the generation of plasma.

5. 2. Multi-Response Optimization using DFA and Optimum Level Prediction using ANN For the multi-response optimization, firstly, the desirability indices (d_i) are calculated using Equations 6 and 7. The parameters JLwS and JLwoS were maximized using Equation 6, whereas PDC and P were minimized using Equation 7. Table 3 shows the d_i of the four response parameters (PDC, JLwS, JLwoS and P) for each experimental trial shown in Table 2 under the column of individual desirability (d_i). Subsequently, the composite desirability indices (CDI) are calculated to take simultaneously optimize the multiple response parameters (Table 3). Finally, the values of CDI are ranked in the descending order from highest to the lowest value to determine the best possible combination of the control parameter to achieve the best performance of the double ring electrode based cold plasma jet. It is observed that, Expt. No. 22 with SV = 5 kV and SF = 25 kHz provides the best performance (highlighted in boldface in Table 3).

To statistically evaluate the factor effects on CDI, its main effect plot is shown in Figure 6(a). It is found that the mean of means of CDI becomes maximum for the control parameter setting of SV = 5 kV and SF = 25 kHz, which is consistent with the results of DFA. Further, a contour plot of CDI is presented in Figure 6(b), wherein its variation is better visualized with respect to the interaction of SV and SF. Here, it is observed that SV < 6 kV results in CDI > 0.6 for almost the entire range of SF. However, for SV > 6 kV, the SF needs to be > 23 kHz to obtain a higher performance output. Also, it can be ascertained that SV = 5 kV and SF = 25 kHz yields the best output since it achieves the maximum CDI (> 0.8).

Regarding the fact that plasma processes require several factors, each of which may have a substantial effect on plasma production. An artificial neural network (ANN) can be used to analyze and predict the impact of such elements with different values operational parameters (supply voltage & supply frequency). For instance, in our study the pulsed power supply cannot be operated at higher voltages such as 7 kV- 10 kV due to physical constraints of the device. Hence, ANN served to be a potent predictive tool for estimating the performance of the device with higher level of accuracy at those operational range (7-10 kV). Also, ANN is highly impactful in analyzing the sensitivity of each of input variables with the performance output such as power consumption, jet length (with/without sleeve).

TABLE 3. Estimated desirability indices using DFA

Expt. No.	Individual desirability (d_i)				CDI	Rank
	PDC	JLwoS	JLwS	P		
1	0.8633	0.0000	0.0000	1.0000	0.0000	46
2	0.8409	0.5373	0.5430	0.9871	0.7015	31
3	0.7897	0.6389	0.6828	0.9511	0.7566	29
4	0.8842	0.8034	0.8120	0.9511	0.8606	7
5	0.7897	0.9036	0.8671	0.9202	0.8687	4
6	0.7260	0.9174	0.8987	0.9626	0.8712	3
7	0.9858	0.5373	0.5430	0.9871	0.7300	30
8	0.9554	0.6389	0.6458	0.9137	0.7747	26
9	0.8633	0.7349	0.7147	0.9137	0.8023	21
10	0.8842	0.8409	0.8499	0.8749	0.8623	6
11	0.7897	0.9306	0.9133	0.8388	0.8662	5
12	0.0000	0.9433	0.9406	0.8967	0.0000	46
13	1.0000	0.6756	0.6458	0.9104	0.7939	24
14	0.9219	0.7349	0.7147	0.8594	0.8031	20
15	0.9554	0.8034	0.8120	0.8211	0.8458	9
16	0.8633	0.9174	0.9133	0.6239	0.8196	18
17	0.8165	0.9554	0.9406	0.6943	0.8448	11
18	0.7598	0.9785	0.9657	0.8633	0.8873	2
19	1.0000	0.7349	0.7147	0.7598	0.7948	23
20	0.9858	0.7825	0.7909	0.7871	0.8325	13
21	0.8633	0.8409	0.8120	0.7922	0.8267	15
22*	**0.9219**	**0.9554**	**0.9657**	**0.7419**	**0.8913**	**1**
23	0.8842	0.9894	0.9889	0.0000	0.0000	46
24	0.5774	1.0000	1.0000	0.6943	0.7957	22
25	0.0913	0.9738	0.9713	0.9298	0.5323	35
26	0.0000	0.9684	0.9801	0.9329	0.0000	46
27	0.0000	0.9636	0.9832	0.9360	0.0000	46
28	0.0000	0.9612	0.9842	0.9391	0.0000	46
29	0.0000	0.9603	0.9845	0.9391	0.0000	46

30	0.0000	0.9601	0.9848	0.9391	0.0000	46
31	0.0000	0.9598	0.9848	0.9391	0.0000	46
32	0.0000	0.9598	0.9848	0.9391	0.0000	46
33	0.0000	0.9623	0.9762	0.9267	0.0000	46
34	0.0000	0.9646	0.9823	0.9329	0.0000	46
35	0.0000	0.9637	0.9837	0.9360	0.0000	46
36	0.0000	0.9625	0.9842	0.9360	0.0000	46
37	0.0000	0.9617	0.9844	0.9391	0.0000	46
38	0.0000	0.9611	0.9847	0.9391	0.0000	46
39	0.0000	0.9607	0.9847	0.9391	0.0000	46
40	0.0000	0.9603	0.9848	0.9391	0.0000	46
41	0.5374	0.9864	0.9834	0.9202	0.8322	14
42	0.3738	0.9842	0.9839	0.9329	0.7623	28
43	0.2475	0.9798	0.9821	0.9360	0.6871	32
44	0.1535	0.9757	0.9811	0.9360	0.6090	33
45	0.0913	0.9724	0.9812	0.9360	0.5344	34
46	0.0000	0.9698	0.9819	0.9360	0.0000	46
47	0.0000	0.9676	0.9828	0.9360	0.0000	46
48	0.0000	0.9657	0.9835	0.9360	0.0000	46
49	0.4894	0.9998	0.9996	0.8071	0.7926	25
50	0.5008	0.9997	0.9995	0.8554	0.8089	19
51	0.5297	0.9995	0.9991	0.8823	0.8266	16
52	0.5607	0.9989	0.9985	0.9002	0.8423	12
53	0.5758	0.9977	0.9971	0.9137	0.8506	8
54	0.5571	0.9956	0.9946	0.9235	0.8448	10
55	0.4941	0.9921	0.9911	0.9298	0.8198	17
56	0.3914	0.9876	0.9873	0.9329	0.7725	27

*The double ring electrode-based argon cold plasma jet operating conditions corresponding to the highest composite desirability.

5. 3. Combinatorial Effects of Supply Voltage and Supply Frequency on the Responses To visually analyze the effects of SV and SF on the output parameters, Figure 7 presents the 3D surface plots of the experimental responses, PDC, JLwS, JLwoS and P with respect to variations in SV and SF. From Figure 7(a), it is observed that, PDC increases from 100 mA to 200 mA with increase in SV from 3.5 kV to 6 kV. However, the effect of SF appears to be more nonlinear with peaks observed near 15 kHz and 25 kHz. The effects on JLwS and JLwoS are more straightforward (Figure 7(b) and (c)). Both JLwS and JLwoS are found to increase with rise in SV and SF, both as individual and interaction effects, yielding a maximum of ≥ 25 mm at the highest values of SV and SF. Another observation is that, SV has a greater influence than SF on both JLwS and JLwoS. The power consumption (P) reaches a minimum of around 0.3 W at the minimum values of both SV and SF (Figure 7(d)). Comparing the effects of the two control parameters, it is found that, SF induces a greater change in P compared to SV.

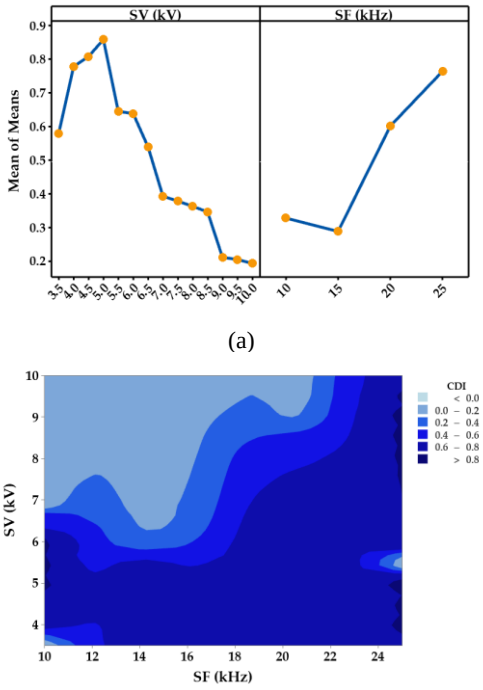

(a)

(b)

Figure 6. (a) Main effect plot and (b) contour plot of composite desirability with respect to SV and SF

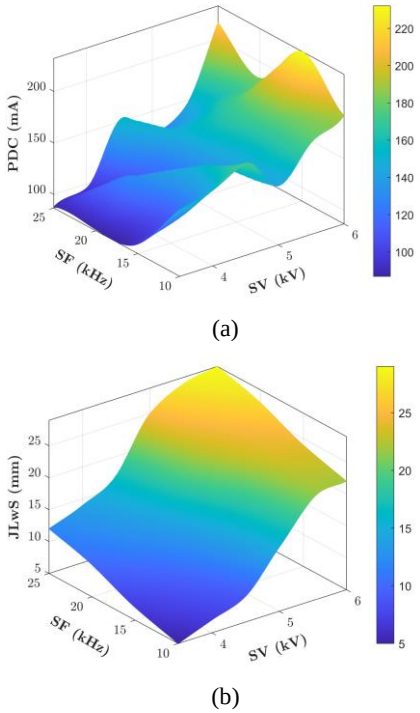

(a)

(b)

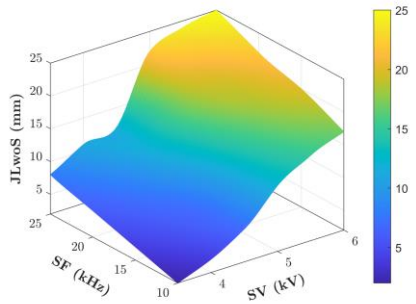

(c)

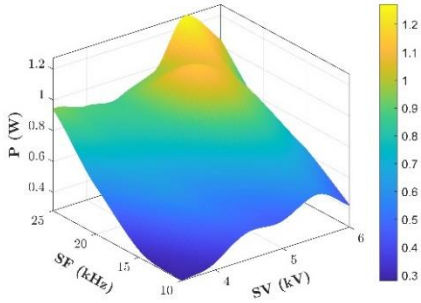

(d)

Figure 7. 3D surface plots showing the contours of responses: (a) PDC, (b) JLwS, (c) JLwoS, (d) P, with respect to the variations in the control parameters: SV and SF

6. CONCLUSIONS

This work presents a modeling and optimization methodology for the performance of the double ring electrode-based argon cold plasma jet using ANN and DFA techniques. The feedforward backpropagation ANN model with '2-8-20-4' topology using the Levenberg-Marquardt algorithm and *tansig* activation function accurately described the experimental responses of pulse discharge current, jet length with and without sleeve, and power consumption ($R^2 > 0.96$) throughout the experimental range: 3.5 kV ≤ SV ≤ 6 kV and 10 kHz ≤ SF ≤ 25 kHz. The optimization using DFA revealed that SV = 5 kV and SF = 25 kHz yielded the best multi-response performance of PDC = 128 mA, JLwS = 25 mm, JLwoS = 22 mm and P = 0.97 W. The interaction effect analysis of composite desirability index showed that SV < 6 kV is advisable for a good performance (CDI > 0.6) for the entire range of 10 kHz ≤ SF ≤ 25 kHz. The analysis of combinatorial effects of SV and SF showed that JLwS and JLwoS become maximum at SV = 6 kV and SF = 25 kHz. PDC becomes minimum near SV = 3.5 kV and 15 kHz ≤ SF ≤ 25 kHz, and P is minimized at SV = 3.5 kV and SF = 10 kHz. The findings of this study demonstrated that the proposed ANN model can be used to evaluate, obtain insights on, and predict the performance of the double ring electrode-based argon cold plasma jet. The results of this study would serve as a benchmark for development of such fundamental predictive models for various types of cold plasma technologies and their optimization.

7. REFERENCES

1. Laroussi M, Lu X. Room-temperature atmospheric pressure plasma plume for biomedical applications. Applied Physics Letters. 2005;87(11). https://doi.org/10.1063/1.2045549
2. Janda M, Martišovitš V, Hensel K, Machala Z. Generation of antimicrobial NO x by atmospheric air transient spark discharge. Plasma Chemistry and Plasma Processing. 2016;36:767-81. https://link.springer.com/article/10.1007/s11090-016-9694-5
3. Klämpfl TG, Isbary G, Shimizu T, Li Y-F, Zimmermann JL, Stolz W, et al. Cold atmospheric air plasma sterilization against spores and other microorganisms of clinical interest. Applied and environmental microbiology. 2012;78(15):5077-82. https://doi.org/10.1128%2FAEM.00583-12
4. Sands BL, Ganguly BN, Tachibana K. A streamer-like atmospheric pressure plasma jet. Applied Physics Letters. 2008;92(15). https://doi.org/10.1063/1.2909084
5. Girard-Lauriault PL, Mwale F, Iordanova M, Demers C, Desjardins P, Wertheimer MR. Atmospheric pressure deposition of micropatterned nitrogen-rich plasma-polymer films for tissue engineering. Plasma Processes and Polymers. 2005;2(3):263-70. http://dx.doi.org/10.1002/ppap.200400092
6. Laroussi M. Low-temperature plasmas for medicine? IEEE Transactions on plasma science. 2009;37(6):714-25. http://dx.doi.org/10.1109/TPS.2009.2017267
7. Kong MG, Kroesen G, Morfill G, Nosenko T, Shimizu T, Van Dijk J, et al. Plasma medicine: an introductory review. new Journal of Physics. 2009;11(11):115012. https://doi.org/10.1088/1367-2630/11/11/115012
8. Morrison KA, Asanbe O, Dong X, Weinstein AL, Toyoda Y, Guevara D, et al. Rapid sterilization of cell phones using a novel portable non-thermal plasma device. Plasma Medicine. 2015;5(1). http://dx.doi.org/10.1615/PlasmaMed.v5.i1.50
9. Mansouri J, Harrisson S, Chen V. Strategies for controlling biofouling in membrane filtration systems: challenges and opportunities. Journal of Materials Chemistry. 2010;20(22):4567-86. https://doi.org/10.1039/B926440J
10. Qi K, Daoud WA, Xin JH, Mak CL, Tang W, Cheung W. Self-cleaning cotton. Journal of Materials Chemistry. 2006;16(47):4567-74. https://doi.org/10.1039/B610861J
11. Deepak GD, Joshi N, Pal U, Prakash R. Electrical characterization of atmospheric pressure dielectric barrier discharge-based cold plasma jet using ring electrode configuration. Laser and Particle Beams. 2016;34(4):615-20. https://doi.org/10.1017/S0263034616000501
12. Weltmann KD, Kindel E, von Woedtke T, Hähnel M, Stieber M, Brandenburg R. Atmospheric-pressure plasma sources: Prospective tools for plasma medicine. Pure and Applied Chemistry. 2010;82(6):1223-37. https://doi.org/10.1351/PAC-CON-09-10-35
13. Von Woedtke T, Reuter S, Masur K, Weltmann K-D. Plasmas for medicine. Physics Reports. 2013;530(4):291-320. https://doi.org/10.1016/j.physrep.2013.05.005
14. Deepak GD, Joshi N, Prakash R. Model analysis and electrical characterization of atmospheric pressure cold plasma jet in pin electrode configuration. AIP Advances. 2018;8(5). https://doi.org/10.1063/1.5023072
15. Divya Deepak G, Joshi N, Pal DK, Prakash R. A low power miniaturized dielectric barrier discharge based atmospheric

pressure plasma jet. Review of Scientific Instruments. 2017;88(1). https://doi.org/10.1063/1.4974101

16. Deepak GD, Joshi NK, Prakash R, Pal U. Electrical characterization of argon and nitrogen based cold plasma jet. The European Physical Journal Applied Physics. 2018;83(2):20801. https://doi.org/10.1051/epjap/2018180057
17. Tanaka H, Ishikawa K, Mizuno M, Toyokuni S, Kajiyama H, Kikkawa F, et al. State of the art in medical applications using non-thermal atmospheric pressure plasma. Reviews of Modern Plasma Physics. 2017;1:1-89. http://dx.doi.org/10.1007/s41614-017-0004-3
18. Lin L, Yan D, Lee T, Keidar M. Self-Adaptive Plasma Chemistry and Intelligent Plasma Medicine. Advanced Intelligent Systems. 2022;4(3):2100112. https://doi.org/10.1063/5.0096789
19. Wan C, Bao H, Chen Z, Lin Q, Liu S, Wu W, et al. The prediction of nitric oxide conversion by dielectric barrier discharge using an artificial neural network model. Journal of the Energy Institute. 2022;101:96-110. https://doi.org/10.1016/j.fochms.2022.100132
20. Nazari RR, Hajizadeh K. Modeling the performance of cold plasma in CO2 splitting using artificial neural networks. AIP Advances. 2022;12(8). http://dx.doi.org/10.1016/j.conbuildmat.2015.07.074
21. Jaddu S, Abdullah S, Dwivedi M, Pradhan RC. Multipin cold plasma electric discharge on hydration properties of kodo millet flour: Modelling and optimization using response surface methodology and artificial neural network–Genetic algorithm. Food Chemistry: Molecular Sciences. 2022;5:100132. https://doi.org/10.1016/j.sciaf.2020.e00413
22. Gholami A, Bonakdari H, Fenjan SA, Akhtari AA. Flow variables prediction using experimental, computational fluid dynamic and artificial neural network models in a sharp bend. International Journal of Engineering, Transaction A: Basics, . 2016;29(1):14-22. 10.5829/idosi.ije.2016.29.01a.03
23. Rajeev D, Dinakaran D, Kanthavelkumaran N, Austin N. Predictions of tool wear in hard turning of AISI4140 steel through artificial neural network, fuzzy logic and regression models. International Journal of Engineering, Transaction A: Basics. 2018;31(1):32-7. 10.5829/ije.2018.31.01a.05
24. Nateghi-A F, Ahmadi MH. Prediction of engineered cementitious composite material properties using artificial neural network. International Journal of Engineering, Transaction B: Applications. 2019;32(11):1534-42. 10.5829/IJE.2019.32.11B.04
25. Harrington EC. The desirability function. Industrial quality control. 1965;21(10):494-8.
26. Derringer G, Suich R. Simultaneous optimization of several response variables. Journal of quality technology. 1980;12(4):214-9. https://doi.org/10.1080/00224065.1980.11980968
27. Devarajaiah D, Muthumari C. Evaluation of power consumption and MRR in WEDM of Ti–6Al–4V alloy and its simultaneous optimization for sustainable production. Journal of the Brazilian Society of Mechanical Sciences and Engineering. 2018;40:1-18. http://dx.doi.org/10.1007/s40430-018-1318-y

8. APPENDIX

The results of various trails conducted to obtain the best accuracy ANN structure (shown in bold) are shown in Table 4. For additional quantitative comparison, the error metrics mean square error (MSE) and mean absolute percentange error (MAPE) have been included:

$$MSE = \frac{1}{n}\sum\left(y - \bar{y}\right)^2 \quad (8)$$

$$MAPE = \frac{100\%}{n}\sum\left|\frac{y - \bar{y}}{y}\right| \quad (9)$$

where, n is the number of data points, y and $\bar{y}$ are the actual and predicted output value, respectively.

TABLE 4. Errors with different ANN structures

Neurons in Layer 1	Neurons in Layer 2	R^2	MSE	MAPE (%)
20	3	0.62	37.119	25.52
18	6	0.76	30.234	19.35
16	8	0.77	27.292	19.01
14	12	0.82	25.632	15.67
12	14	0.91	20.246	9.13
10	16	0.90	20.842	10.02
8	**20**	**0.97**	**16.062**	**3.62**
6	20	0.89	21.423	10.34
3	20	0.71	31.357	21.35

Persian Abstract

چکیده

پلاسمای فشار اتمسفر سرد (CAP) یک فناوری بسیار قوی و تاثیرگذار است که هم برای کاربردهای تکنولوژیکی و هم برای کاربردهای زیست پزشکی اجرا شده است. این مقاله بر اجرای شبکه عصبی مصنوعی (ANN) برای پلاسمای فشار اتمسفر سرد مبتنی بر الکترود دو حلقه جدید متمرکز است که برای کاربرد آن در زمینه زیست پزشکی فقط در منطقه تخلیه درخشش عمل می‌کند. ANN ذاتاً به تجسم پارامترهای خروجی مؤثر مانند جریان دبی اوج، توان مصرفی، طول جت (با آستین) و طول جت (بدون آستین) برای مجموعه پارامترهای ورودی ولتاژ و فرکانس منبع تغذیه با استفاده از مدل یادگیری ماشین کمک می‌کند. قابلیت مدل ANN با پیش‌بینی پارامترهای خروجی CAP فراتر از محدوده تجربی نشان داده می‌شود. در نهایت، تنظیمات بهینه ولتاژ تغذیه و فرکانس منبع تغذیه با استفاده از رویکرد تابع مطلوبیت ترکیبی تعیین می‌شود تا همزمان جریان تخلیه پیک، طول جت (با آستین) و طول جت (بدون آستین) را به حداکثر برساند و مصرف برق را به حداقل برساند.